Effect of non-ideal power take-off on the electric output power of a wave energy converter under suboptimal control

M. F. Pettersen & O. B. Fosso
Department of Electric Power Engineering
Norwegian University of Science and Technology, Trondheim, Norway

P. B. Garcia-Rosa
SINTEF Energy Research
Trondheim, Norway

M. Molinas
Department of Engineering Cybernetics
Norwegian University of Science and Technology, Trondheim, Norway

ABSTRACT: This work investigates how the physical limitations and losses of an electric power take-off (PTO) system affect the production of power for a wave energy converter (WEC) under suboptimal control strategies. The damping of the PTO system is either continuously tuned to the time-varying wave excitation force frequency, which is referred to as passive control (PC), or tuned to the mean centroid frequency of the spectrum, which is referred to as passive loading (PL). The time-varying frequency is estimated by the Hilbert-Huang transform (HHT) method. Numerical simulations with the wave-to-wire model of a WEC including a non-ideal PTO show that the limitations and losses of the system modify the output power for both control strategies, when compared to the ideal PTO case. Furthermore, the benefit of applying the time-varying damping obtained from HHT for certain types of wave spectra differs significantly from the cases when only the hydrodynamic model with an ideal PTO system is considered. While for an ideal PTO system, the greatest improvement of PC over PL is obtained for wideband spectra, this behaviour is not observed when the non-ideal PTO is considered.

1 INTRODUCTION

Different control schemes have been proposed to improve the energy absorption of wave energy converters (WECs) for a variety of operating conditions. Although the performance of most of these control schemes have been evaluated through the use of numerical simulation models with ideal power take-off (PTO) systems, a few numerical studies have considered non-ideal PTOs in the control problem formulation, e.g., Bacelli et al. (2015), Sánchez et al. (2015).

Additionally, the impact of PTO limitations and losses on the energy output of reactively controlled WECs have been studied, e.g., for the Lifesaver WEC (Sjolte et al. 2013) and generic non-ideal PTO systems (Falcão and Henriques 2015, Genest et al. 2014, Tedeschi et al. 2011). Optimal hydrodynamic control, and reactive control, imply bidirectional power flow, which requires highly efficient power take-off (PTO) systems. For a Western Atlantic site and a generic WEC, Genest et al. (2014) have shown that while reactive control can improve the WEC mean annual power absorption by a factor of 10 with an ideal PTO, such a factor is reduced to 4 for actuators with 90% efficiency and further reduced to 2 for actuators with 80% efficiency. If the efficiencies are below 50%, the losses are so high that the use of this control strategy is not meaningful.

Similar behavior has been observed for the wave energy converter Lifesaver. Due to large accumulated average losses and limited efficiency of the generator, Sjolte et al. (2013) have shown that the electric PTO system of this WEC has limited potential for increased production by reactive control. Simulation results have indicated that an annual increase in energy production of only 1% could be obtained when compared to the passive loading (PL) case.

This paper will investigate the impact of non-ideal PTO system on the electric output power of a passively controlled WEC. To this end, the hydrodynamic model of an oscillating body is connected to an

all-electric PTO system like the system of Lifesaver (Sjolte et al. 2013). We consider the PTO damping of the WEC to be either tuned to time-frequency estimations obtained from the Hilbert-Huang transform (HHT) method or to the mean centroid frequency of the excitation force spectrum.

Previous studies using HHT on the control problem formulation (Garcia-Rosa et al. 2017, Garcia-Rosa et al. 2019) have focused only on hydrodynamic models, where the WEC performance under passive and reactive control has been measured in terms of absorbed power and PTO rating. Non-ideal PTO systems have not yet been considered for control schemes based on HHT. In this study, the WEC performance under the HHT passive control will be evaluated in terms of electric output power by using a fully coupled wave-to-wire model, which includes the physical limitations and efficiency of the PTO.

2 WAVE-TO-WIRE DYNAMIC MODELLING

The WEC considered in this paper is a single oscillating point absorber, moving only in heaving motion. The body is a vertical cylinder, and it is connected to an electric PTO system like the PTO of the wave energy converter Lifesaver (Sjolte et al. 2013).

2.1 *Time-series of the wave elevation*

Irregular waves are modelled as a finite number of sinusoidal waves with different amplitudes, frequencies and phases. The elevation of an irregular wave can be calculated as (Ricci et al. 2008)

$$\zeta(t) = \sum_{n=1}^{N} \sqrt{2S(\omega_n)\omega_n}\,\sin(\omega_n t + \phi_n)\,, \tag{1}$$

where $S(\omega)$ characterizes the wave spectrum, ω_n and ϕ_n are the angular frequency and random phase of the n-th wave component, respectively.

Various mathematical models can be used to describe the wave spectrum. Here, we consider the Ochi-Hubble spectrum, which is a 6-parameter wave spectrum decomposed into two parts: one containing low frequency components of the wave energy (remotely generated swells) and the second including high frequency components (local wind waves) (Ochi & Hubble 1976). The wave spectrum can be expressed as

$$S(\omega) = \frac{1}{4}\sum_{j=1}^{2} \frac{\left[(\lambda_j + 0.25)\,\omega_{m_j}\right]^{\lambda_j}}{\Gamma(\lambda_j)} \frac{H_{s_j}^2}{\omega^{4\lambda_j+1}} e^{-\frac{(\lambda_j+0.25)\,\omega_{m_j}^4}{\omega^4}}, \tag{2}$$

which has two sets of a three-parameter spectrum. Each set consists of a spectral shape parameter λ_j, a significant wave height H_{s_j} and a modal or peak frequency ω_{m_j}.

2.2 *Hydrodynamic model*

Using Newton's second law of motion and assuming linear hydrodynamic theory, the motion of the floating body can be described as

$$m\ddot{x}(t) = f_e(t) + f_r(t) + f_s(t) + f_p(t)\,, \tag{3}$$

where $\ddot{x}$(t) is the body acceleration, m is the body mass, $f_e(t)$ is the excitation force, $f_r(t)$ is the radiation force, $f_s(t)$ is the hydrostatic force, and $f_p(t)$ is the PTO force.

The hydrostatic force is the resultant force between the gravitational force and the force due to buoyancy when the body moves from its equilibrium position. As a result, the hydrostatic force can be calculated as

$$f_s(t) = -Sx(t)\,, \tag{4}$$

where S the hydrostatic stiffness and x is the body displacement.

The excitation force is the force acting on the body as it is held fixed in incident waves. The excitation force is expressed as

$$f_e(t) = \int_{-\infty}^{\infty} h_e(t-\tau)\zeta(\tau)d\tau, \tag{5}$$

where the inverse Fourier transform of the excitation force transfer function $H_e(\omega)$ can be found by

$$h_e(t) = \frac{1}{2\pi}\int_{-\infty}^{\infty} H_e(\omega)e^{i\omega t}d\omega. \tag{6}$$

The radiation force is the force due to waves generated by the body motion. It can be expressed as (Cummins 1962)

$$-f_r(t) = m_r(\infty)\ddot{x} + \int_0^t h_r(t-\tau)\dot{x}(\tau)\,d\tau\,, \tag{7}$$

where $m_r(\infty)$ is the added mass coefficient at infinite frequency, and the integration kernel $h_r(t-\tau)$, known as the fluid memory term (Greenhow & White 1997), is given by

$$h_r(t-\tau) = \frac{2}{\pi}\int_0^{\infty} B_r(\omega)\cos(\omega(t-\tau))d\omega\,, \tag{8}$$

where B_r is the radiation damping.

The PTO force is defined as

$$f_p(t) = -B_p(t)\dot{x}(t), \tag{9}$$

where $B_p \in \mathbb{R}_+$ represents the PTO damping and $\dot{x}(t)$ is the velocity of the floating body.

The mean absorbed power for a time interval T is calculated as

$$P_a(t) = -\frac{1}{T}\int_0^T f_p(t)\dot{x}(t)dt\,. \tag{10}$$

2.3 *Electric PTO model*

The electric PTO system of Lifesaver generates electric power through a winch that is connected to the mooring line, as illustrated in Figure 1. In order to maintain a continuous rope tension, the generator needs to operate as a motor whenever the device performs a downward motion, and then, power flows from the grid to the WEC. The generator produces power only during the upwards motion of the device (Sjolte et al. 2013).

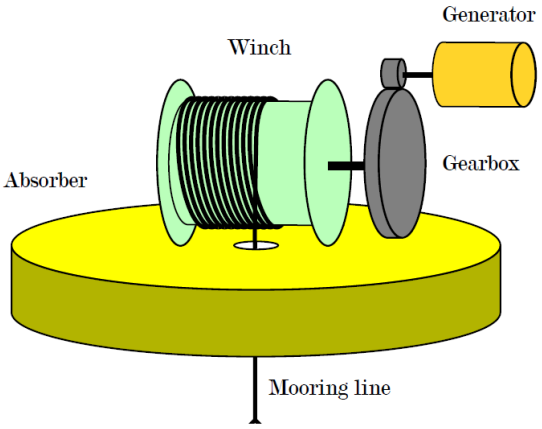

Figure 1: PTO of Lifesaver (Sjolte et al. 2013).

The stand-alone system consists of the following components: 28-pole surface-mounted permanent magnet synchronous machine (SMPMSM); inverter/rectifiers; ultra-capacitor bank; DC-link charger; battery charger; brake charger and dump resistor. In the synchronous reference frame, the mathematical model of a SMPMSM drive system is commonly expressed as (Vas 1990):

$$u_{ds} = R_s i_{ds} + \frac{d}{dt}\left(L_s i_{ds} + \Psi_{PM}\right) - \omega_r L_s i_{qs}\,, \tag{11}$$

$$u_{qs} = R_s i_{qs} + \frac{d}{dt}\left(L_s i_{qs}\right) - \omega_r\left(L_s i_{qs} + \Psi_{PM}\right)\,, \tag{12}$$

where u_{ds} and u_{qs} are the stator d- and q-axis voltages, i_{ds} and i_{qs} are the stator d- and q-axis currents, R_s and L_s denote the stator resistance and inductance, and Ψ_{PM} is the permanent magnet flux linkage. The rotor angular speed of the generator ω_r is calculated from the hydrodynamic model as

$$\omega_r(t) = \frac{n_p}{2}\rho_g\,\dot{x}(t)\,, \tag{13}$$

where ρ_g is the angular to gear ratio, and n_p is the number of poles of the generator.

The electromagnetic torque of the generator is calculated as

$$T_e(t) = \frac{3}{2}\frac{n_p}{2}\Psi_{PM} i_{qs}(t)\,. \tag{14}$$

From (11) and (12), a cross coupling between the d- and q-axis voltage occurs. This can be avoided by using a feedforward technique, where the reference voltages are defined as

$$v_{ds}(t) = u_{ds}(t) + \omega_r L_s i_{qs}(t)\,, \tag{15}$$

$$v_{qs}(t) = u_{qs}(t) - \omega_r L_s i_{ds}(t) - e_q(t)\,, \tag{16}$$

where e_q is the induced voltage in the q-axis. By applying these equations to (11) and (12), two independent first-order equations in the synchronous reference frame are obtained. Then, the transfer function from the current i to the voltage v is given by

$$\frac{i(s)}{v(s)} = \frac{\dfrac{1}{R_s}}{1 + \dfrac{L_s}{R_s}s}\,, \tag{17}$$

and the current controller can be implemented as illustrated in the block diagram in Figure 2.

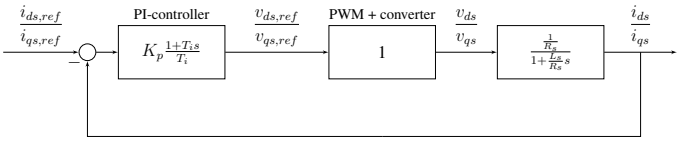

Figure 2: Block diagram of the current controller.

The transfer function for the PWM and converter is set to unity because it is assumed that the voltage from the converter follows the reference voltage perfectly. As a result, the simulation time is significantly reduced and there is no need for a filter in the system (Sjolte et al. 2013).

In order to ensure that the limitations of the PTO are not exceeded, torque control is required. The reference torque is calculated using the machinery force from the hydrodynamic model:

$$T_{e,ref}(t) = \frac{1}{\rho_g} f_p(t)\,, \tag{18}$$

where f_p is defined by (9). Thus, the reference for the q-current is given by

$$i_{qs,ref}(t) = \frac{T_{e,ref}(t)}{\dfrac{3}{2}n_p\Psi_{PM}}\,. \tag{19}$$

The actual references for q- and d-axis currents used for torque control are updated according to $i_{qs,ref}$ values (19) and the generator characteristics, as summarized below (Sjolte et al. 2013):

1. If $I_{qs,min} < i_{qs,ref} < I_{qs,max}$, then $i_{qs,ref} = i_{qs,ref}$ and $i_{ds,ref} = 0$;
2. If $I_{qs,min} > i_{qs,ref}$ and $\omega_r < \omega_{rm}$, then $i_{qs,ref} = I_{qs,min}$ and $i_{ds,ref} = 0$;
3. If $i_{qs,ref} > I_{qs,max}$ and $\omega_r < \omega_{rm}$, then $i_{qs,ref} = I_{qs,max}$ and $i_{ds,ref} = 0$;

4. Otherwise, if $\omega_r > \omega_{rm}$, then field weakening is necessary.

$I_{qs,min}, I_{qs,max}$ are, respectively, minimum and maximum q-axis currents and ω_{rm} is the field weakening speed.

During field weakening, the d- and q-axis currents are decided through a method described by Ching-Tsai Pan and Jenn-Horng Liaw (2005). The method is based on using the current and voltage constraints of the SMPMSM drive system to calculate the real-time upper and lower q-axis current bounds. Using the generator characteristics, the field weakening speed ω_{rm} (in rad/s) is given by

$$\omega_{rm} = \frac{-2R_s I_{max}\Psi_{PM} + \sqrt{(2R_s I_{max}\Psi_{PM})^2 - 4(\Psi_{PM}^2 + L_s^2 I_{max}^2)(R_s^2 I_{max}^2 - V_{max}^2)}}{2(\Psi_{PM}^2 + L_s^2 I_{max}^2)} \tag{20}$$

The detailed properties of the generator and converter are not exactly known. However, based on provided information on the efficiency at a number of operating points, a polynomial expression for the combined generator and converter losses has been determined by Sjolte et al. (2013). The power losses (P_l) are calculated as a function of the generator torque T_e and the angular speed of the rotor ω_r (in rpm):

$$|P_l| = a_1 T_e^4 + a_2 T_e^2 + a_3|\omega_r| + a_4\omega_r^2 + a_5|\omega_r T_e| + a_6|\omega_r|T_e^2 \,. \tag{21}$$

3 POWER TAKE-OFF DAMPING

3.1 *Constant frequency tuning*

For passive loading, the PTO damping is set to a constant value, i.e. $B_p(t) = B_p$, for any time t, where B_p can be adjusted according to a chosen tuning frequency. For an incoming regular wave, i.e. wave consisting of only one frequency, the optimal PTO damping is calculated as (Falnes 2002)

$$B_p = \sqrt{B_r(\omega)^2 + \left[\omega(m + m_r(\omega)) - \frac{S}{\omega}\right]^2} \,. \tag{22}$$

A challenge with PL is to define the tuning frequency for real ocean waves and irregular waves, as these waves do not consist of a single frequency. Usually, the energy frequency or the peak frequency of the wave spectrum is defined as the tuning frequency. Then, the PTO damping can be tuned following an hourly basis (sea state variations), a monthly basis (seasonal variations) or an annually basis.

In any practical application studies, tuning the PTO damping to the frequency of the waves will require an estimation of the frequency. In Garcia-Rosa et al. (2019), simulation studies indicate that the extended Kalman filter, which is a state observer commonly used in real-time applications, estimates the mean centroid frequency of the excitation force spectrum (ω_{1,f_e}). Thus, in this paper, PL uses this frequency for tuning the damping.

The mean centroid frequency (ω_1) is a statistical parameter of the wave spectrum given by the spectral moments m_1 and m_0 as $\omega_1 = m_1/m_0$. Spectral moments of order n are calculated as

$$m_n = \int_0^\infty \omega^n S(\omega) d\omega \,. \tag{23}$$

3.2 *Time-frequency tuning using the Hilbert-Huang Transform*

For a passive control (PC) scheme that tunes the PTO on a wave-by-wave basis, $B_p(t)$ can be calculated as

$$B_p(t) = \sqrt{B_r(\hat{\omega}_d)^2 + \left[\hat{\omega}_d(m + m_r(\hat{\omega}_d)) - \frac{S}{\hat{\omega}_d}\right]^2} \,, \tag{24}$$

where $\hat{\omega}_d(t)$ is the estimated time-domain frequency of the wave excitation force. The reason the excitation force is used rather than the wave elevation is because, in this way, some of the high frequency content of the wave elevation is filtered by $H_e(\omega)$. As in Garcia-Rosa et al. (2017), the frequency in this paper is estimated by the HHT method.

HHT is a two-step method for analyzing nonstationary and nonlinear signals. Firstly, the empirical mode decomposition (EMD) decomposes the original signal into intrinsic mode functions (IMFs). Secondly, the Hilbert transform (HT) is used on each IMF component to estimate the instantaneous frequency and amplitude (Huang et al. 1998). The EMD identifies the different frequencies of the signal $f_e(t)$ through the process of sifting, as summarized in the following algorithm:

Step 0: Set $i = 1$ and $r(t) = f_e(t)$;

Step 1: Identify local maxima and minima in $r(t)$;

Step 2: Create upper and lower envelopes defined from the corresponding maxima and minima using cubic spline interpolation;

Step 3: Calculate the mean of the envelopes $m(t)$;

Step 4: Subtract the mean from the signal, $h(t) = r(t) - m(t)$;

Step 5: If $h(t)$ can be classified as an IMF, go to the next step. Otherwise, set $r(t) = h(t)$ and repeat the process from 1;

Step 6: Set $c_i(t) = r(t)$. Calculate $r(t) = r(t) - c_i(t)$, set $i = 2, ..., N$ and repeat the process from 1. Define the IMF components as $c_1(t)$, ..., $c_N(t)$ and the residue as $r(t)$.

After the EMD has been completed, the IMF components are given in a sequential order from the highest frequency component to the lowest. Next, the energy of each IMF signal is calculated in order to locate the IMF with the highest energy content (Garcia-Rosa et al. 2017),

$$E_{c_i} = \int_0^T \mid c_i(t) \mid^2 dt\,, \tag{25}$$

where $c_i(t)$ is the i-th IMF component. The IMF with the highest energy content is the dominant component $c_d(t)$. Finally, the HT is applied to $c_d(t)$,

$$v_d(t) = \frac{1}{\pi} P\Big\{ \int_{-\infty}^{\infty} \frac{c_d(\tau)}{t-\tau} d\tau \Big\}\,, \tag{26}$$

where P is the Cauchy principal value. Then, the dominant IMF component can be expressed as an analytical signal,

$$z_d(t) = c_d(t) + j v_d(t) = \hat{a}_d(t) e^{j \int \hat{\omega}_d(t) dt}, \tag{27}$$

where $\hat{a}_d(t)$ is the instantaneous amplitude,

$$\hat{a}_d(t) = \sqrt{c_d^2(t) + v_d^2(t)}\,, \tag{28}$$

and $\hat{\omega}_d(t)$ is the instantaneous frequency,

$$\hat{\omega}_d(t) = \frac{d}{dt} \arctan\left(\frac{v_d(t)}{c_d(t)}\right)\,. \tag{29}$$

The instantaneous frequency (29) is used as the tuning frequency in the PTO damping calculation (24).

4 NUMERICAL SIMULATIONS

In order to evaluate the effect of a non-ideal PTO on passively controlled WECs, a comparison of the electric output power is considered for the cases when the PTO damping is tuned to

- a constant frequency of the excitation force spectrum, which is referred to as the PL approach. Here, the mean centroid frequency, ω_{1,f_e}, is considered;
- frequency estimated by HHT, $\hat{\omega}_d(t)$, which is referred to as the PC approach.

Firstly, a comparison of the results considering only the hydrodynamic model (Section 2.2) is performed. In this case, an ideal PTO system is assumed, and the mean absorbed power $\bar{P}_a$ is the output power.

4.1 *Simulation Parameters*

Ochi-Hubble spectra (2) are generated from the real wave data of the Belmullet wave energy test site used in Garcia-Rosa et al. (2017). The spectral shape parameters $(\lambda_1, \lambda_2, H_{s_1}, H_{s_2}, \omega_{m_1}, \omega_{m_2})$ are set to mimic three sea states from that paper: S1, S2, and S6 (which is renamed as S3 here). The simulation interval is $T = 30$ min with sampling frequency of 1.28 Hz. The

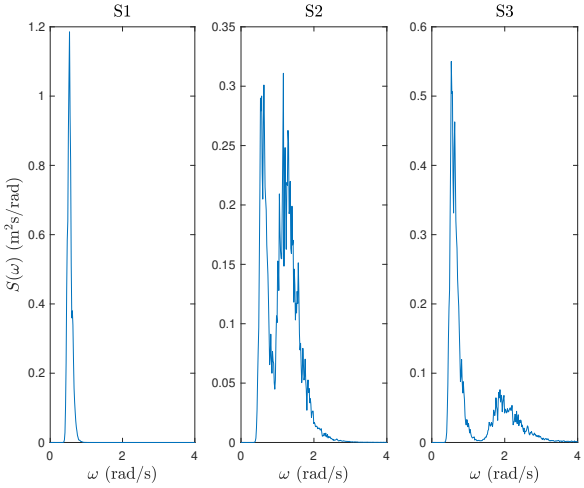

Figure 3: Simulated wave spectra S1, S2 and S3.

spectral densities of the excitation force for the given sea states are shown in Figure 4. Comparing the wave and excitation force spectra, it can be seen that some of the high frequency content in the wave spectra have been filtered out by $H_e(\omega)$. The heaving cylinder used

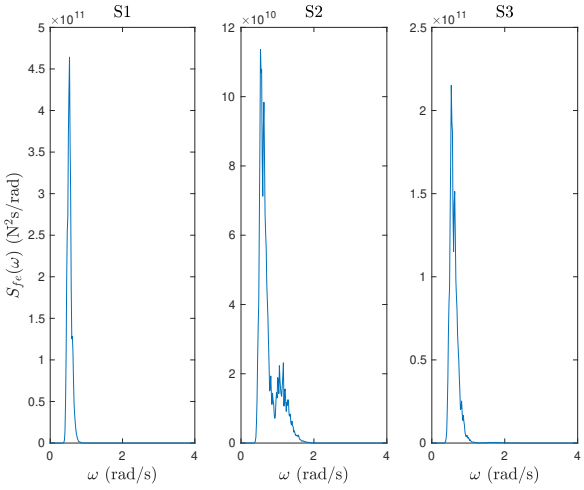

Figure 4: Spectral density of the excitation force for sea states S1, S2 and S3.

in Garcia-Rosa et al. (2017) is also considered here. The main specifications of the electric PTO system are listed in Table 1, and the generator characteristics are shown in Table 2 (Sjolte et al. 2013).

By assuming a simplified converter bridge with PWM, the time constant T_i in the PI-controller (Fig. 2) becomes equal to the armature time constant, and the gain K_p is set as 0.8.

Table 1: Main PTO specifications.

Property	Value
DC-bus voltage, V_{max}	600 V
DC-bus current, I_{max}	481.2679 A
Angular to linear gear ratio, ρ_g	38.5 1/m
PTO maximum force	100 kN
PTO minimum force	10 kN

Table 2: Generator characteristics.

Property	Value
Number of poles, n_p	28
Stator resistance, R_s	0.038 Ω
Stator inductance, L_s	1.4 mH
Permanent magnet flux linkage, Ψ_{PM}	0.257 Wb
Maximum q-current, $I_{qs,max}$	481.2679 A
Minimum q-current, $I_{qs,min}$	48.1268 A
Field weakening speed, ω_{rm}	561.1284 rpm

4.2 *Hydrodynamic model*

For the hydrodynamic model with an ideal PTO system, the ratios between $\bar{P}_a$ with PC and $\bar{P}_a$ with PL are shown in Table 3.

Table 3: Ratios between $\bar{P}_a(PC)$ and $\bar{P}_a(PL)$.

Ratio	S1	S2	S3
$\bar{P}_a(PC)/\bar{P}_a(PL)$	1.01	1.32	1.03

For all sea states, the output power is greater for PC than for PL tuned with ω_{1,f_e}, where the advantage of using PC and HHT frequency estimation is more evident for S2, a sea state with mixed waves spread over a wide band of frequencies. These results agree with previous results shown in Garcia-Rosa et al. (2017). Figure 5 illustrates the energy absorbed for both schemes.

4.3 *Wave-to-wire model*

As explained in Section 2.3, the generator produces power only during the upwards motion of the device. Thus, to verify the effect of the control methods on the output electric power, the average electric power ($\bar{P}_e$) is split into positive ($\bar{P}_{e+}$) and negative ($\bar{P}_{e-}$) components, following the upward and downward motions of the body.

Figure 6 illustrates the generated energy for PL and PC over the 30-min simulation interval in sea states S1, S2 and S3. As expected, a comparison with Figure 5 shows that the energy output levels for the fully coupled ware-to-wire are lower, due to PTO limitations and losses. Furthermore, a different behaviour is observed when PL and PC are compared for each sea state, and the advantage of using PC with HHT is more evident in S3. Thus, the greatest improvements of PC over PL, previously associated with wideband

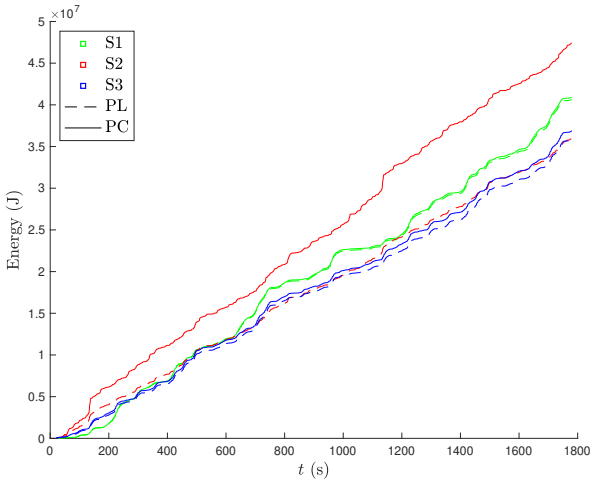

Figure 5: Absorbed energy for PL and PC over a 30-min simulation (hydrodynamic model with ideal PTO).

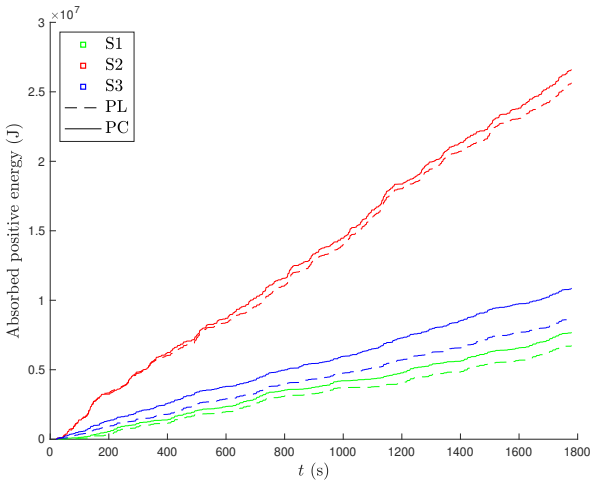

Figure 6: Generated energy for PL and PC over a 30-min simulation (wave-to-wire model with non-ideal PTO).

spectra, have not been observed for the fully wave-to-wire model. This is further indicated in Table 4, which shows all the ratios of average eletric power and the ratio of power losses between PC and PL.

Although PC results in more production of power than PL, it also results in at least twice as much negative power than PL, i.e. more power is flowing from the grid to the WEC when PC is applied, as shown in Table 4 (third line). As a consequence, the average electric power ($\bar{P}_e$) becomes almost the same for PL and PC.

From Table 4 (last line), it can be seen that PL results in higher power losses than PC. The power losses depend on both the generator speed ω_r and generator torque T_e, as indicated by (21). In the polynomial expression, the torque values are raised to the fourth power, and then, the losses become higher for cases with higher torque.

The losses are calculated on the basis of copper losses here, but in a SMPMSM machine, iron losses are also a significant fraction of the total losses (Meier 2002). It is also important to note that continuously modifying the operating region of the generator may cause other losses related to wear and tear over time,

Table 4: Ratios between average electric powers, and ratios between power losses.

Ratio	S1	S2	S3
$\bar{P}_e(PC)/\bar{P}_e(PL)$	1.02	0.9	0.99
$\bar{P}_{e+}(PC)/\bar{P}_{e+}(PL)$	1.14	1.04	1.25
$\bar{P}_{e-}(PC)/\bar{P}_{e-}(PL)$	1.51	1.8	2.22
$\bar{P}_l(PC)/\bar{P}_l(PL)$	0.97	0.8	0.9

which are not considered in this study.

Figures 7-11 show samples of time-series simulation for the generator speed, generator torque, PTO damping and electric currents for both PL and PC.

The generator speed is very similar for both control schemes (Fig. 7), showing only slightly differences at the peaks. However, the generator torque (Fig. 8) exhibits more pronounced differences when the control schemes are compared, since the torque control reference is directly proportional to the PTO damping (Fig. 9), which oscillates over a wide range for PC. For both control schemes, the generator torque frequently switches between its maximum and minimum values, i.e. the electric PTO system works at the boundary of its capacity. However, PL results in higher torque values than PC, which explains PL exhibits higher power losses.

Due to the proportionality between the generator torque and the q-axis current (14), PL gives higher i_{qs} values than PC, as illustrated in Figure 11. Additionally, it can be noticed S2 is the only sea state that results in field weakening (Fig. 10), which is caused when the generator speed is higher than $\omega_{r,m}$ (Fig. 7). The benefit of using the time-varying damping is reduced for sea state S2 when compared to S1 and S3.

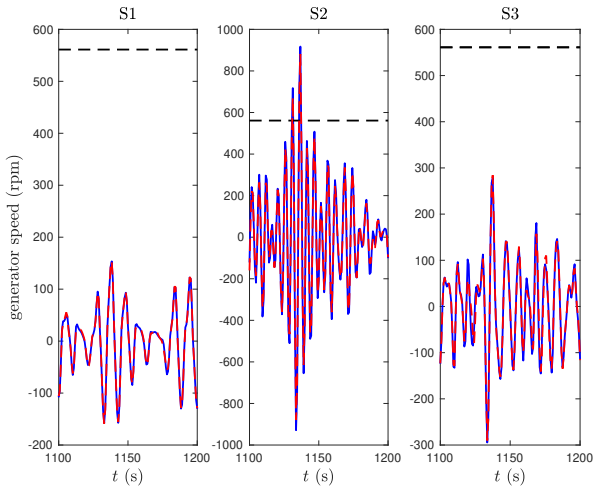

Figure 7: Generator speed for the time interval 1000 s and 1200 s for PL (dashed red) and PC (solid blue). Black dashed line is the field weakening speed ω_{rm}.

5 CONCLUSION

For an ideal PTO system, the greatest improvement of passive control with HHT frequency estimations

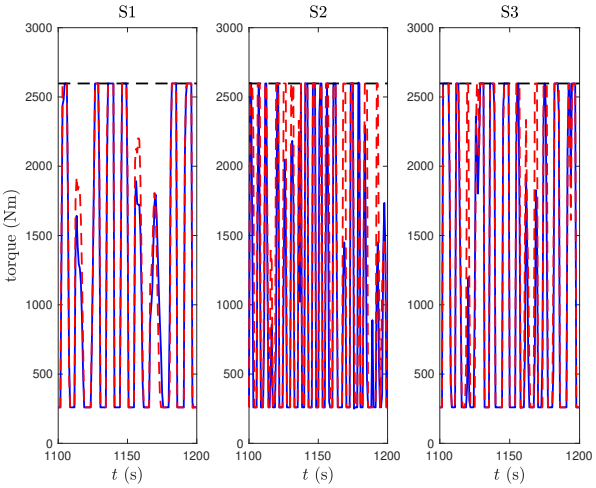

Figure 8: Generator torque for the time interval 1000 s and 1200 s for PL (dashed red) and PC (solid blue). Black dashed line is the maximum generator torque.

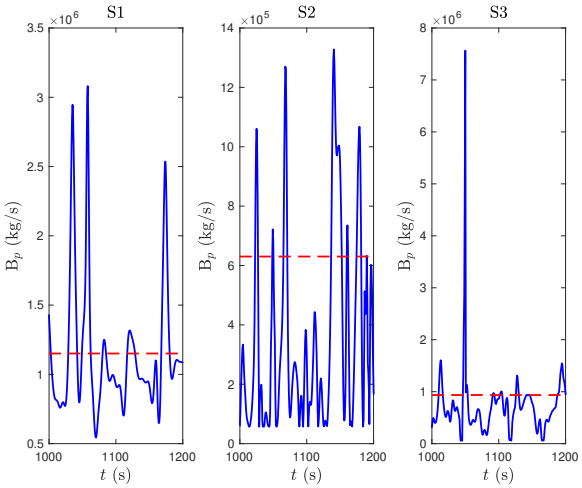

Figure 9: PTO damping for the time interval 1000 s and 1200 s for PL (dashed red) and PC (solid blue).

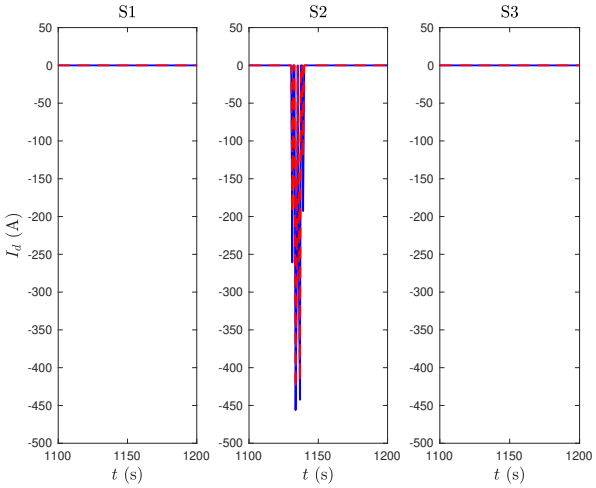

Figure 10: D-axis current for the time interval 1000 s and 1200 s for PL (dashed red) and PC (solid blue).

over passive loading is obtained for wideband spectra. This behavior is not observed when the non-ideal electric PTO of the Lifesaver WEC is considered. For instance, for the two-peak wideband spectrum considered here, the field weakening region of the generator is activated, and the benefit of using a time-varying

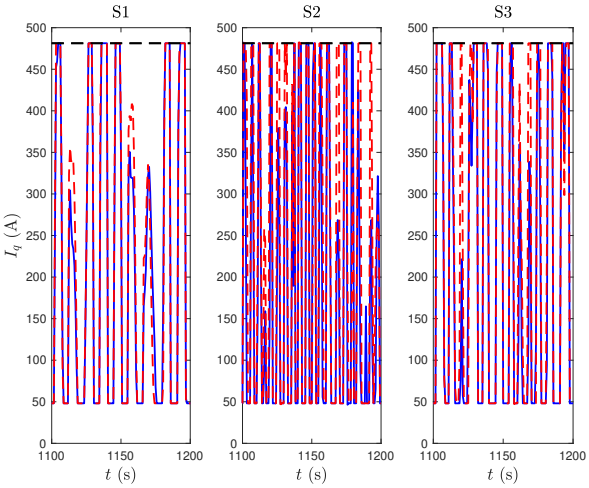

Figure 11: Q-axis current for the time interval 1000 s and 1200 s for PL (dashed red) and PC (solid blue). Black dashed line is the maximum q-current $I_{qs,max}$.

damping is significantly reduced when compared to the ideal case. However, for sea states S1 and S3, the benefit of using HHT is increased. Future works will further investigate this behavior.

Simulation results indicate that the WEC generates more electric power with PC than with PL, even with the non-ideal PTO and the inherent losses and limitations of the system. However, PC requires significantly more power from the grid to operate correctly during the downwards motion of the floating body. The considered WEC generates power only during upwards motion of the body.

Additionally, higher power losses are observed with PL than with PC. Higher losses are derived from higher generator torques, and hence, higher stator currents. The torque control reference is directly proportional to the PTO damping, which is constant for PL and oscillates over a wide range following the frequency bandwidth of the sea state for PC. In the wave-to-wire model, the power losses are found only through the stator copper losses, even though iron losses are also significant in a SMPMSM machine.

REFERENCES

Bacelli, G., R. Genest, & J. V. Ringwood (2015). Nonlinear control of flap-type wave energy converter with a non-ideal powert ake-off system. *Annual Reviews in Control 40*, 116–216.

Ching-Tsai Pan & Jenn-Horng Liaw (2005). A robust field-weakening control strategy for surface-mounted permanent-magnet motor drives. *IEEE Transactions on Energy Conversion 20*(4), 701–709.

Cummins, W. E. (1962). The impulse response function and ship motions. *Schiffstechnik 47*(9), 101–109.

Falcão, A. F. O. & J. C. C. Henriques (2015). Effect of non-ideal power take-off efficiency on performance of single- and two-body reactively controlled wave energy converters. *J. Ocean Eng. Mar. Energy 1*, 273–286.

Falnes, J. (2002). *Ocean Waves and Oscillating Systems: Linear Interaction including Wave-Energy Extraction*. Cambridge University Press.

Garcia-Rosa, P. B., G. Kulia, J. V. Ringwood, & M. Molinas (2017). Real-time passive control of wave energy converters using the hilbert-huang transform. In *IFAC-PapersOnLine Volume 50(1), Proc. of the 20th IFAC World Congress*, pp. 14705–14710.

Garcia-Rosa, P. B., J. V. Ringwood, O. B. Fosso, & M. Molinas (2019). The impact of time–frequency estimation methods on the performance of wave energy converters under passive and reactive control. *IEEE Trans. on Sustainable Energy 10*(4), 1784–1792.

Genest, R., F. Bonnefoy, A. H. Clément, & A. Babarit (2014). Effect of non-ideal power take-off on the energy absorption of a reactively controlled one degree of freedom wave energy converter. *Applied Ocean Research 48*, 236–243.

Greenhow, M. & S. P. White (1997). Optimal heave motion of some axisymmetric wave energy devices in sinusoidal waves. *Applied Ocean Research 19*(3), 141–159.

Huang, N. E., Z. Shen, S. R. Long, M. C. Wu, H. H. Shih, Q. Zheng, N.-C. Yen, C. C. Tung, & H. H. Liu (1998). The empirical mode decomposition and the Hilbert spectrum for nonlinear and non-stationary time series analysis. *Proc. Royal Society London 454*, 903–995.

Meier, S. (2002). Theoretical design of surface-mounted permanent magnet motors with field weakening capability. Master's thesis, Royal Institute of Technology.

Ochi, M. K. & E. N. Hubble (1976). Six-parameter wave spectra. In *Coastal Engineering 1976*, pp. 301–328.

Ricci, P., J.-B. Saulnier, A. Falcao, & M. Pontes (2008, 01). Time-domain models and wave energy converters performance assessment. In *Proceedings of the International Conference on Offshore Mechanics and Arctic Engineering - OMAE*, Volume 6.

Sjolte, J., C. Sandvik, E. Tedeschi, & M. Molinas (2013, 07). Exploring the potential for increased production from the wave energy converter lifesaver by reactive control. *Energies 6*, 3706–3733.

Sánchez, E. V., R. H. Hansen, & M. M. Kramer (2015). Control performance assessment and design of optimal control to harvest ocean energy. *IEEE Journal of Oceanic Engineering 40*(1), 15–26.

Tedeschi, E., M. Carraro, M. Molinas, & P. Mattavelli (2011). Effect of control strategies and power take-off efficiency on the power capture from sea waves. *IEEE Trans. on Energy Conversion 26*(4), 1088—1098.

Vas, P. (1990). *Vector control of AC machines*, Volume 22 of *Monographs in electrical and electronic engineering*. Oxford: Clarendon Press.